PHOTONICS Research

Enhancing the expansion of a plasma shockwave by crater-induced laser refocusing in femtosecond laser ablation of fused silica

Qingsong Wang,[1] Lan Jiang,[1,*] Jingya Sun,[1] Changji Pan,[1] Weina Han,[1] Guoyan Wang,[1] Hao Zhang,[1] Costas P. Grigoropoulos,[2] and Yongfeng Lu[3]

[1]Laser Micro/Nano Fabrication Laboratory, School of Mechanical Engineering, Beijing Institute of Technology, Beijing 100081, China
[2]Laser Thermal Laboratory, Department of Mechanical Engineering, University of California, Berkeley, California 94720, USA
[3]Department of Electrical and Computer Engineering, University of Nebraska-Lincoln, Lincoln, Nebraska 68588-0511, USA
*Corresponding author: jianglan@bit.edu.cn

Received 13 July 2017; revised 21 August 2017; accepted 23 August 2017; posted 24 August 2017 (Doc. ID 302410); published 20 September 2017

The dynamics of plasma and shockwave expansion during two femtosecond laser pulse ablation of fused silica are studied using a time-resolved shadowgraph imaging technique. The experimental results reveal that during the second pulse irradiation on the crater induced by the first pulse, the expansion of the plasma and shockwave is enhanced in the longitudinal direction. The plasma model and Fresnel diffraction theory are combined to calculate the laser intensity distribution by considering the change in surface morphology and transient material properties. The theoretical results show that after the free electron density induced by the rising edge of the pulse reaches the critical density, the originally transparent surface is transformed into a transient high-reflectivity surface (metallic state). Thus, the crater with a concave-lens-like morphology can tremendously reflect and refocus the latter part of the laser pulse, leading to a strong laser field with an intensity even higher than the incident intensity. This strong refocused laser pulse results in a stronger laser-induced air breakdown and enhances the subsequent expansion of the plasma and shockwave. In addition, similar shadowgraphs are also recorded in the single-pulse ablation of a concave microlens, providing experimental evidence for the enhancement mechanism.

OCIS codes: (320.7100) Ultrafast measurements; (140.3390) Laser materials processing; (140.3440) Laser-induced breakdown.

https://doi.org/10.1364/PRJ.5.000488

1. INTRODUCTION

The nonlinear non-equilibrium process of femtosecond laser–material interactions has drawn intense attention over the last couple of decades due to the unique properties of ultrafast pulse duration and ultrahigh power density [1–4]. This process involves multiscale physico-chemical phenomena ranging from laser energy absorption and phase change to material removal [5,6], which are fundamentally different from those induced by a conventional long pulsed laser [7]. Among these phenomena, the dynamics of plasma and shockwave are crucial, not only for understanding the fundamental interaction mechanisms [8–10] but also for controlling structure formation and corresponding applications [11–13].

Recently, a time-resolved shadowgraph imaging technique has emerged as an effective method for revealing the dynamics of femtosecond laser–material interactions. Numerous studies have investigated the effects of laser parameters (e.g., laser fluence [14], pulse duration [14,15], and temporal [16] and spatial shaping [17]), material properties [18–20], and ablation environments [21,22] on the dynamics of plasma expansion and shockwave evolution. Boueri and colleagues compared the early-stage expansion of plasma and shockwaves induced by femtosecond and nanosecond lasers by analyzing the expansion velocity and plume density [14,15]. Zhang and colleagues observed the multiple material ejection and shockwave generation outside or inside different materials, and revealed the thermal and nonthermal mechanisms during intense femtosecond laser irradiation [18,19]. Hu *et al.* emphasized the restriction of liquid on the diffusion of the ejected material and attenuation of the shockwave [21]. However, these studies were mainly focused on the dynamic behavior under single-pulse irradiation. In the fabrication of numerous structures, irradiating the same location with multiple pulses is necessary [23,24]. Under multiple pulse irradiation, the material properties and morphologies changed by the previous pulses can significantly affect the interactions of successive pulses with the material.

For example, multiple pulses can induce a transition of damage mechanisms and ablation morphology due to prior laser-induced defects [25,26]. Moreover, the initial structures, such as laser-induced periodic surface structures and micro-craters, have been demonstrated to reshape the incident laser in terms of reflection, scattering, absorption, and transmission [27–30]. The reshaped laser intensity is believed to affect the evolution of laser-induced plasma and subsequent shockwave expansion. However, few studies have investigated this issue, and the underlying physics remains unclear.

In this paper, we present a time-resolved study of the plasma and shockwave evolution during two-pulse (pulse separation exceeding 1 s) ablation of fused silica in atmospheric air. The experimental results reveal that the expansion of the plasma and shockwave is enhanced in the longitudinal direction during the second pulse irradiation. This enhancement is interpreted in terms of a laser-induced air breakdown assisted by the crater with its concave-lens-like morphology. The interpretation is supported by a theoretical calculation of the reflected intensity focused by the crater by considering the change in transient material properties during laser irradiation. To further confirm this observation, we present experimental evidence on single-pulse ablation of a concave microlens formed by femtosecond laser-enhanced chemical etching, during which the enhancement can also be observed.

2. EXPERIMENT

Figure 1 shows the schematic of the pump–probe experimental setup. A commercial Ti:sapphire femtosecond laser regenerative amplifier (Spitfire, Spectral Physics Inc.) with a pulse duration of 50 fs and central wavelength of 800 nm was employed as the laser source. The original pulse was divided into pump and probe pulses by a beam splitter. The pump beam was focused by a 5× objective lens (NA = 0.15, Olympus, Inc.) normally onto the surface of commercial polished fused silica in atmospheric air, and the diameter was 12.6 μm. The pump energy was regulated using a variable neutral density filter. The probe beam, with an orientation perpendicular to the pump beam, was frequency doubled by a beta barium borate (BBO) crystal, and then used to illuminate the ablated area. The transmitted shadowgraph of plasma and shockwave was imaged onto a charge-coupled device (CCD) by a 20× objective lens

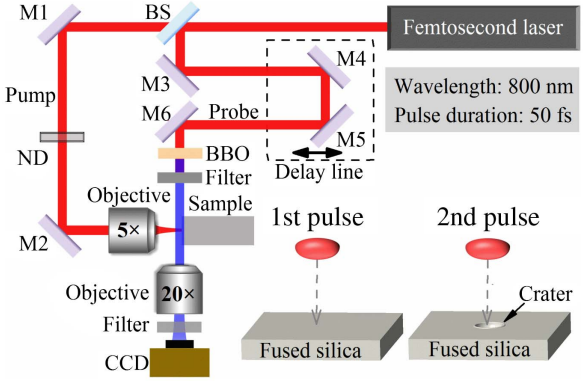

Fig. 1. Schematic of the pump–probe experimental setup. BS, beam splitter; M, mirror; ND, variable neutral density filter.

(NA = 0.45, Olympus, Inc.). A 400 nm bandpass filter before the CCD was used to suppress background illumination from the residual 800 nm laser and plasma radiation. The probe delays were controlled by an optical delay line. To study the dynamics of two-pulse ablation, we recorded a sequence of shadowgraphs during the first and second pulse ablation at different probe delays. Background subtraction was employed to obtain sharper images of the recorded shadowgraphs [17]. After experiments, the ablation morphology was characterized with an atomic force microscope (AFM, Dimension edge, Bruker Inc.).

3. RESULTS AND DISCUSSION

Figure 2 shows the time-resolved images of the femtosecond laser ablation dynamics of fused silica after the first and second pulse irradiation with a fluence of 13.75 J/cm^2. Typical images show laser-induced plasma on the picosecond timescale [Figs. 2(a) and 2(d)] and evident shockwave on the nanosecond timescale [Figs. 2(b) and 2(e)], consistent with previous studies [15,19]. Comparing the plasma and shockwave evolution induced by the second pulse with those induced by the first pulse, we surprisingly identified a needle-like protuberance on the top of the plasma induced by the second pulse [Fig. 2(d)], and it became more pronounced for the subsequent shockwave expansion [Fig. 2(e)], whereas no obvious changes in the plasma and shockwave profiles were observed in the radial direction. The shockwave expansion distances were measured. At 16 ns the propagation distance in the longitudinal direction was 86.2 and 100.5 μm for the first and second pulse ablations, respectively, whereas they remained nearly constant at approximately 39.0 μm in the radial direction. These results indicate that the expansion of the plasma and shockwave was enhanced in the longitudinal direction during the second pulse ablation.

After such intense femtosecond laser irradiation, craters were formed on the surface of fused silica and were characterized with AFM. A smooth and slightly elliptical crater with a diameter of 8.52 μm and a depth of 0.32 μm was obtained after the first pulse ablation [Fig. 2(c)], and the crater volume was estimated to be 14.32 μm^3. After the second pulse irradiation, the diameter, depth, and volume of the crater increased to 8.91 μm, 0.63 μm, and 28.71 μm^3, respectively [Fig. 2(f)]. Thus, the ablation depth and volume induced by the second pulse were 0.31 μm and 14.39 μm^3, respectively, which remained nearly unchanged compared with those induced by the first pulse.

The enhancement was also investigated under laser irradiation with different fluences. Figure 3 compares the shadowgraphs of the shockwaves induced by the first and second pulse at a probe delay of 16 ns, with fluences of 10.8, 19.2, and 40.1 J/cm^2. With the first pulse ablation, a protuberance emerged on the top of the shockwave front as the laser fluence increased [Figs. 3(a)–3(c)]. As has been frequently discussed in previous studies [14,15,31], this structure can be attributed to laser-induced air breakdown, which induces a plasma channel with a lower refractive index. The shockwave expansion was thus accelerated in the longitudinal direction, leading to the formation of a protuberance on the shockwave front. For the second pulse ablation, expansion enhancement was evident for all the applied fluences [Figs. 3(d)–3(f)]. In the case of

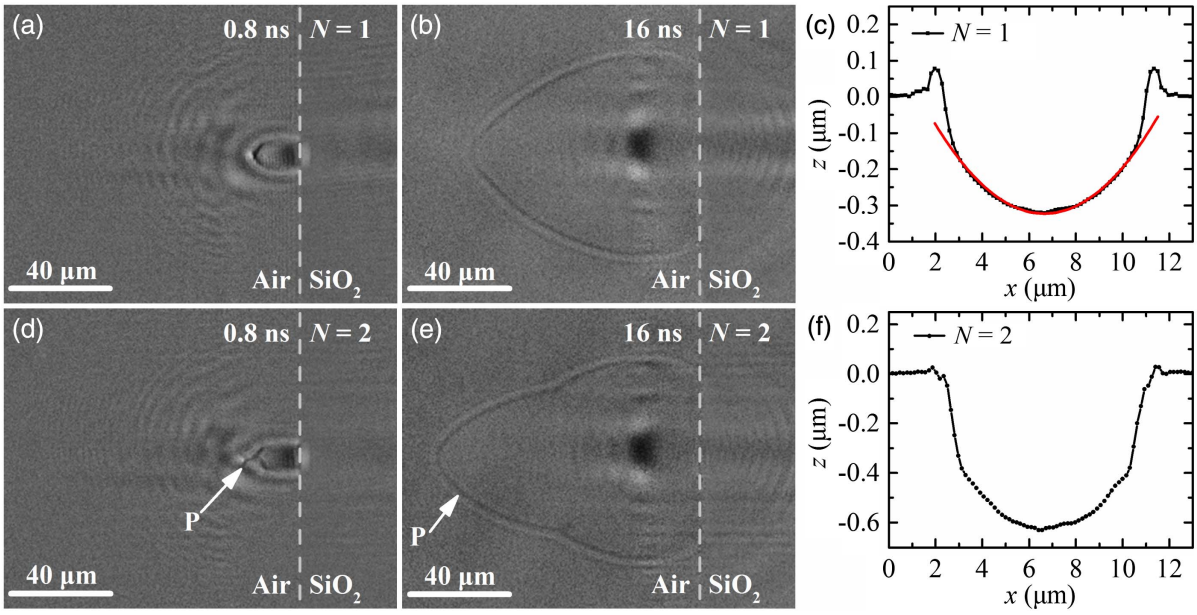

Fig. 2. Time-resolved shadowgraphs of the plasma and shockwave generated by femtosecond laser irradiation on fused silica with a laser fluence of 13.75 J/cm^2. (a), (b) Images recorded after the first pulse ($N = 1$); (d), (e) images recorded after the second pulse ($N = 2$). P indicates the protuberance on the top of the plasma and shockwave front. (c), (f) AFM morphologies of the crater cross section after the first and second pulse ablation. The red line in (c) is the parabolic curve fitting for the cross section with a radius of curvature of 44 μm.

10.8 J/cm^2, the semi-elliptic shockwave front induced by the first pulse [Fig. 3(a)] was deformed by the second pulse, and a protuberance emerged on the top of the shockwave front [Fig. 3(d)].

The expansion of the plasma and shockwave is driven by laser ablation and affected by the surrounding environment [14,21,31]. The aforementioned results demonstrate that the ablation rate and shockwave expansion in the radial direction remained unchanged during two-pulse ablation, thus eliminating laser ablation as the dominant cause of the expansion enhancement. On the other hand, the shockwave induced by the second pulse [Fig. 2(e)] had similar morphology to that induced by a single pulse with higher pulse energy accompanied by air breakdown [Fig. 3(c)]. Therefore, the shockwave enhancement can be explained by the crater-assisted laser-induced air breakdown. During intense femtosecond laser ablation of fused silica, free electrons are generated via nonlinear ionization [6], and the density can reach 10^{21}–10^{22} cm^{-3}. According to

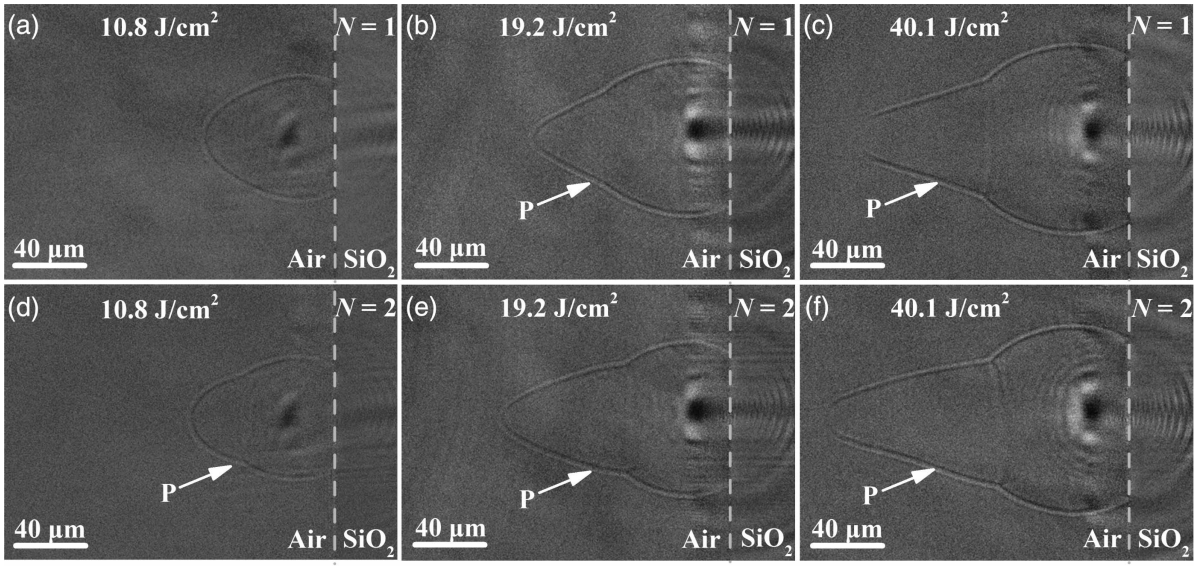

Fig. 3. Shadowgraphs of the plasma and shockwave generated by femtosecond laser irradiation on fused silica with laser fluences of 10.8, 19.2, and 40.1 J/cm^2. (a)–(c) Images recorded after the first pulse ($N = 1$), (d)–(f) images recorded after the second pulse ($N = 2$). P indicates the protuberance on the top of the plasma and shockwave front. The probe delay is 16 ns.

the Drude model [32,33], the great change in free electron density substantially alters the originally transparent surface into a transient high-reflectivity surface [34]. Thus, the intense femtosecond laser is tremendously reflected into the air, facilitating air excitation. For two-pulse ablation, a crater is formed on the initial fresh surface by the first pulse, and this crater can be then employed as a concave microlens [30] to reflect and refocus the second femtosecond laser due to its transient high surface reflectivity during laser irradiation. Therefore, the reflected pulse has higher intensity and can induce stronger air breakdown. The air plasma channel accelerates the expansion of the plasma and shockwave in the longitudinal direction, enhancing the formation of the protuberance on the plasma and shockwave front.

The corresponding value of the reflected laser intensity during two-pulse ablation was estimated by combining the plasma model [34,35] and Fresnel diffraction theory [36,37]. The plasma model can calculate the free electron generation, transient material properties, and incident and reflected laser intensity distributions. Briefly, the free electron generation can be calculated as

$$\frac{\partial n_e(t,r,z)}{\partial t} = \alpha_i I(t,r,z) n_e(t,r,z) + \delta_N [I(t,r,z)]^N - \frac{n_e(t,r,z)}{\tau}, \quad (1)$$

where t is the time, r is the distance to the Gaussian beam axis, z is the depth from the surface, $n_e(t,r,z)$ is the free electron density, α_i is the impact ionization constant, $I(t,r,z)$ is the incident laser intensity, δ_N is the cross section of N-photon absorption, and τ is the decay time constant. The free electrons change the spatially and temporally dependent dielectric function of the material $\varepsilon(t,r,z)$, which can be expressed by Drude model:

$$\varepsilon(t,r,z) = \varepsilon_s - \frac{\omega_p^2}{\omega[\omega + i/\tau_e(t,r,z)]}, \quad (2)$$

where ε_s is the intrinsic dielectric constant of fused silica, ω is the laser frequency, $\tau_e(t,r,z)$ is the effective electron collision time, and ω_p is the plasma frequency, which can be expressed as

$$\omega_p = \sqrt{n_e e^2/(m^* \varepsilon_0)}, \quad (3)$$

where e is the electron charge, m^* is the effective mass of the electron, and ε_0 is the vacuum permittivity. Therefore, the reflected laser intensity is expressed as

$$I_r(t,r) = I(t,r) R(t,r), \quad (4)$$

where $I(t,r)$ is the incident laser intensity on the surface and $R(t,r)$ is the transient reflectivity at the surface, which is determined by the Fresnel expression:

$$R(t,r) = \frac{[f_1(t,r,0)-1]^2 + f_2^2(t,r,0)}{[f_1(t,r,0)+1]^2 + f_2^2(t,r,0)}, \quad (5)$$

$$f_1(t,r,0) + i f_2(t,r,0) = [\varepsilon(t,r,0)]^{1/2}, \quad (6)$$

where $f_1(t,r,0)$ is the normal refractive index and $f_2(t,r,0)$ is the extinction coefficient. Figures 4(a) and 4(b) show the evolution of the surface reflectivity and the incident and reflected laser intensities under the first pulse irradiation with a fluence of 13.75 J/cm^2. After the free electron density (n_e) induced by the rising edge of the pulse reached the critical density (n_{cr}), the surface reflectivity increased rapidly and the maximum transient reflectivity was higher than 0.9. Hence, the latter part of the laser pulse was mainly reflected into the air, and the maximum reflected laser intensity exceeded 2.3×10^{14} W/cm^2 [Fig. 4(a)].

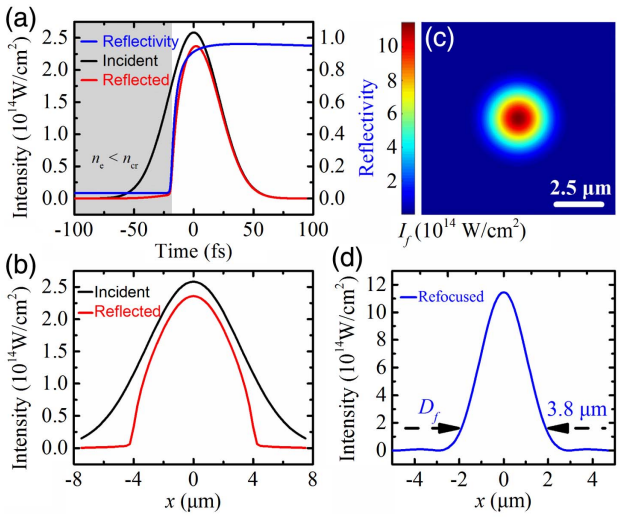

Fig. 4. Calculation of the refocused laser intensity. (a) Time dependence of surface reflectivity, and incident and reflected laser intensity at the beam center ($x = 0$) during the first pulse irradiation, (b) spatial distributions of the incident and reflected laser intensity at time zero, at which the peak intensity arrives during the first pulse irradiation, (c) refocused laser intensity distribution at the refocused focal plane at time zero during the second pulse irradiation, (d) cross section of the refocused laser intensity distribution at time zero. The incident laser fluence is 13.75 J/cm^2.

In the case of estimation of the transient refocused laser intensity during the second pulse irradiation, we assumed for simplicity that the microlens surface had the same transient reflectivity as the fresh surface. Thus, the transient refocused intensity can be calculated with Fresnel diffraction theory by considering the spatial distribution of the transient reflected intensity [Fig. 4(b)]:

$$I_f(t,x_r,y_r,z_r) = \left| \frac{\exp(ikz_r)}{i\lambda z_r} \iint A_r(t,x,y) \times \exp\left[-ik\frac{x^2+y^2}{2f} + ik\frac{(x_r-x)^2+(y_r-y)^2}{2z_r} \right] dx dy \right|^2, \quad (7)$$

where $I_f(t,x_r,y_r,z_r)$ is the refocused intensity, k is the wave vector, λ is the laser wavelength, $A_r(t,x,y)$ is the field amplitude of the reflected laser, and f is the focal length of the crater. Under the focusing conditions with a focal length of 22 μm deduced from its AFM morphology [Fig. 2(c)], the focal diameter was reduced to 3.8 μm [Figs. 4(c) and 4(d)], thereby enabling a calculated transient focused laser intensity that was much higher than the reflected intensity from the flat surface. For example, the transient focused laser intensity for the peak intensity arrival was estimated to be 11.45×10^{14} W/cm^2,

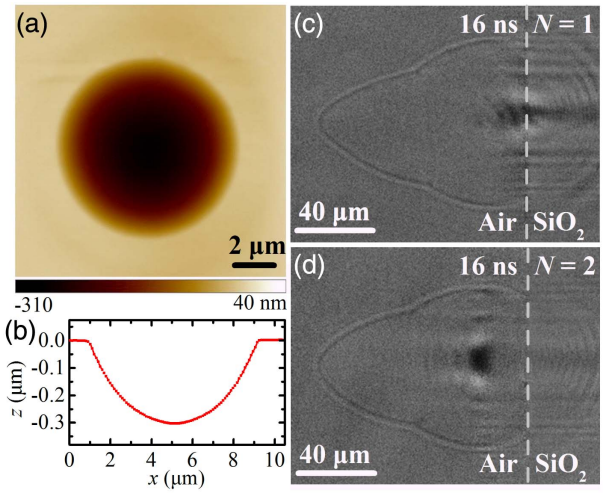

Fig. 5. (a), (b) AFM morphology of the microlens fabricated by single femtosecond laser irradiation with a fluence of 4.5 J/cm^2, followed by 5% HF etching for 90 min, (c) shadowgraph of the shockwave induced by single-pulse ablation of a concave microlens ($N = 1$), (d) shadowgraph of the shockwave induced by the second pulse ablation of flat fused silica ($N = 2$). The fluence is 13.75 J/cm^2.

which was even higher than the peak intensity of the incident laser (2.58×10^{14} W/cm^2). Such a high refocused laser intensity was expected to enhance the air breakdown, and thus accelerate the plasma and shockwave expansion.

The enhancement mechanism was further demonstrated experimentally by shadowgraph imaging of the femtosecond laser ablation of a preformed microlens without laser-induced debris and defects. The silica microlens was fabricated by femtosecond laser-enhanced hydrofluoric acid (HF) etching [38]. Figures 5(a) and 5(b) show the fabricated microlens with a diameter of 8.45 μm and a depth of 0.305 μm, which is similar to the crater induced by a single pulse with a fluence of 13.75 J/cm^2. Figure 5(c) shows the shadowgraph of a laser-induced shockwave at a probe delay of 16 ns after single-pulse irradiation on a fresh microlens with a fluence of 13.75 J/cm^2. For comparison, the shadowgraph of the shockwave induced by the second pulse ablation of flat fused silica at a probe delay of 16 ns with the same fluence is shown in Fig. 5(d). As expected, a protuberance appeared on the front of the shockwave induced by single-pulse ablation of the microlens, which was in agreement with the morphology of the shockwave induced by the second pulse ablation of flat fused silica.

4. CONCLUSION

We have experimentally and theoretically revealed the crater-enhanced expansion of the plasma and shockwave during two femtosecond laser pulse ablation of fused silica. During the second pulse irradiating the crater induced by the first pulse, the expansion of the plasma and shockwave was enhanced in the longitudinal direction but remained unchanged in the radial direction. This phenomenon was attributed to the crater-assisted laser-induced air breakdown, which accelerated the expansion of the plasma and shockwave in the longitudinal direction. This study demonstrates the significant role of multiple pulses in laser-induced plasma evolution, and may improve prospects for understanding and regulating laser–material interactions during multiple-pulse irradiation.

Funding. National Natural Science Foundation of China (NSFC) (51605029, 91323301).

REFERENCES

1. M. Schultze, E. M. Bothschafter, A. Sommer, S. Holzner, W. Schweinberger, M. Fiess, M. Hofstetter, R. Kienberger, V. Apalkov, V. S. Yakovlev, M. I. Stockman, and F. Krausz, "Controlling dielectrics with the electric field of light," Nature **493**, 75–78 (2013).
2. C. Kerse, H. Kalaycıoğlu, P. Elahi, B. Cetin, D. K. Kesim, Ö. Akcaalan, S. Yavas, M. D. Asik, B. Öktem, H. Hoogland, R. Holzwarth, and F. Ö. Ilday, "Ablation-cooled material removal with ultrafast bursts of pulses," Nature **537**, 84–88 (2016).
3. B. Öktem, I. Pavlov, S. Ilday, H. Kalaycıoğlu, A. Rybak, S. Yavaş, M. Erdoğan, and F. Ö. Ilday, "Nonlinear laser lithography for indefinitely large-area nanostructuring with femtosecond pulses," Nat. Photonics **7**, 897–901 (2013).
4. A. P. Joglekar, H. H. Liu, E. Meyhöfer, G. Mourou, and A. J. Hunt, "Optics at critical intensity: applications to nanomorphing," Proc. Natl. Acad. Sci. USA **101**, 5856–5861 (2004).
5. R. R. Gattass and E. Mazur, "Femtosecond laser micromachining in transparent materials," Nat. Photonics **2**, 219–225 (2008).
6. P. Balling and J. Schou, "Femtosecond-laser ablation dynamics of dielectrics: basics and applications for thin films," Rep. Prog. Phys. **76**, 036502 (2013).
7. B. C. Stuart, M. D. Feit, A. M. Rubenchik, B. W. Shore, and M. D. Perry, "Laser-induced damage in dielectrics with nanosecond to subpicosecond pulses," Phys. Rev. Lett. **74**, 2248–2251 (1995).
8. R. Stoian, D. Ashkenasi, A. Rosenfeld, and E. E. B. Campbell, "Coulomb explosion in ultrashort pulsed laser ablation of Al_2O_3," Phys. Rev. B **62**, 13167–13173 (2000).
9. X. Zhao and Y. C. Shin, "Coulomb explosion and early plasma generation during femtosecond laser ablation of silicon at high laser fluence," J. Phys. D **46**, 335501 (2013).
10. C. Kalupka, J. Finger, and M. Reininghaus, "Time-resolved investigations of the non-thermal ablation process of graphite induced by femtosecond laser pulses," J. Appl. Phys. **119**, 153105 (2016).
11. S. Noël and J. Hermann, "Reducing nanoparticles in metal ablation plumes produced by two delayed short laser pulses," Appl. Phys. Lett. **94**, 053120 (2009).
12. A. Heins and C. L. Guo, "Shock-induced concentric rings in femtosecond laser ablation of glass," J. Appl. Phys. **113**, 223506 (2013).
13. B. Xia, L. Jiang, X. Li, X. Yan, and Y. Lu, "Mechanism and elimination of bending effect in femtosecond laser deep-hole drilling," Opt. Express **23**, 27853–27864 (2015).
14. M. Boueri, M. Baudelet, J. Yu, X. Mao, S. S. Mao, and R. Russo, "Early stage expansion and time-resolved spectral emission of laser-induced plasma from polymer," Appl. Surf. Sci. **255**, 9566–9571 (2009).
15. X. Zeng, X. L. Mao, R. Greif, and R. E. Russo, "Experimental investigation of ablation efficiency and plasma expansion during femtosecond and nanosecond laser ablation of silicon," Appl. Phys. A **80**, 237–241 (2005).
16. T. Y. Choi, D. J. Hwang, and C. P. Grigoropoulos, "Femtosecond laser induced ablation of crystalline silicon upon double beam irradiation," Appl. Surf. Sci. **197–198**, 720–725 (2002).
17. Y. Yu, L. Jiang, Q. Cao, B. Xia, Q. Wang, and Y. Lu, "Pump-probe imaging of the fs-ps-ns dynamics during femtosecond laser Bessel beam drilling in PMMA," Opt. Express **23**, 32728–32735 (2015).
18. N. Zhang, X. Zhu, J. Yang, X. Wang, and M. Wang, "Time-resolved shadowgraphs of material ejection in intense femtosecond laser ablation of aluminum," Phys. Rev. Lett. **99**, 167602 (2007).
19. H. Hu, X. Wang, H. Zhai, N. Zhang, and P. Wang, "Generation of multiple stress waves in silica glass in high fluence femtosecond laser ablation," Appl. Phys. Lett. **97**, 061117 (2010).
20. B. D. Strycker, M. M. Springer, A. J. Traverso, A. A. Kolomenskii, G. W. Kattawar, and A. V. Sokolov, "Femtosecond-laser-induced

shockwaves in water generated at an air-water interface," Opt. Express **21**, 23772–23784 (2013).
21. H. Hu, T. Liu, and H. Zhai, "Comparison of femtosecond laser ablation of aluminum in water and in air by time-resolved optical diagnosis," Opt. Express **23**, 628–635 (2015).
22. Z. Wu, X. Zhu, and N. Zhang, "Time-resolved shadowgraphic study of femtosecond laser ablation of aluminum under different ambient air pressures," J. Appl. Phys. **109**, 053113 (2011).
23. B. Xia, L. Jiang, X. Li, X. Yan, W. Zhao, and Y. Lu, "High aspect ratio, high-quality microholes in PMMA: a comparison between femtosecond laser drilling in air and in vacuum," Appl. Phys. A **119**, 61–68 (2015).
24. J. Bonse and J. Krüger, "Pulse number dependence of laser-induced periodic surface structures for femtosecond laser irradiation of silicon," J. Appl. Phys. **108**, 034903 (2010).
25. R. Stoian, A. Rosenfeld, D. Ashkenasi, I. V. Hertel, N. M. Bulgakova, and E. E. B. Campbell, "Surface charging and impulsive ion ejection during ultrashort pulsed laser ablation," Phys. Rev. Lett. **88**, 097603 (2002).
26. H. Varel, M. Wähmer, A. Rosenfeld, D. Ashkenasi, and E. E. B. Campbell, "Femtosecond laser ablation of sapphire: time-of-flight analysis of ablation plume," Appl. Surf. Sci. **127–129**, 128–133 (1998).
27. J. R. V. de Aldana, C. Méndez, and L. Roso, "Saturation of ablation channels micro-machined in fused silica with many femtosecond laser pulses," Opt. Express **14**, 1329–1338 (2006).
28. M. Huang, F. Zhao, Y. Cheng, N. Xu, and Z. Xu, "Origin of laser-induced near-subwavelength ripples: interference between surface plasmons and incident laser," ACS Nano **3**, 4062–4070 (2009).
29. L. S. Jiao, E. Y. K. Ng, H. Y. Zheng, and Y. L. Zhang, "Theoretical study of pre-formed hole geometries on femtosecond pulse energy distribution in laser drilling," Opt. Express **23**, 4927–4934 (2015).
30. J. Zhang, R. Drevinskas, M. Beresna, and P. G. Kazansky, "Polarization sensitive anisotropic structuring of silicon by ultrashort light pulses," Appl. Phys. Lett. **107**, 041114 (2015).
31. H. Zhang, F. Zhang, X. Du, G. Dong, and J. Qiu, "Influence of laser-induced air breakdown on femtosecond laser ablation of aluminum," Opt. Express **23**, 1370–1376 (2015).
32. B. C. Stuart, M. D. Feit, S. Herman, A. M. Rubenchik, B. W. Shore, and M. D. Perry, "Nanosecond-to-femtosecond laser-induced breakdown in dielectrics," Phys. Rev. B **53**, 1749–1761 (1996).
33. K. Zhang, L. Jiang, X. Li, X. Shi, D. Yu, L. Qu, and Y. Lu, "Femtosecond laser pulse-train induced breakdown in fused silica: the role of seed electrons," J. Phys. D **47**, 435105 (2014).
34. L. Jiang and H. L. Tsai, "Repeatable nanostructures in dielectrics by femtosecond laser pulse trains," Appl. Phys. Lett. **87**, 151104 (2005).
35. L. Jiang and H. L. Tsai, "Plasma modeling for ultrashort pulse laser ablation of dielectrics," J. Appl. Phys. **100**, 023116 (2006).
36. F. He, H. Xu, Y. Cheng, J. Ni, H. Xiong, Z. Xu, K. Sugioka, and K. Midorikawa, "Fabrication of microfluidic channels with a circular cross section using spatiotemporally focused femtosecond laser pulses," Opt. Lett. **35**, 1106–1108 (2010).
37. T. Wang, L. Jiang, X. Li, J. Hu, Q. Wang, S. Ye, H. Zhang, and Y. Lu, "Controllable anisotropic wetting characteristics on silicon patterned by slit-based spatial focusing of femtosecond laser," Opt. Express **24**, 25732–25741 (2016).
38. F. Chen, H. Liu, Q. Yang, X. Wang, C. Hou, H. Bian, W. Liang, J. Si, and X. Hou, "Maskless fabrication of concave microlens arrays on silica glasses by a femtosecond-laser-enhanced local wet etching method," Opt. Express **18**, 20334–20343 (2010).